DR-BUDDI: Diffeomorphic Registration for Blip Up-Down Diffusion Imaging

M. Okan Irfanoglu[1,2], Pooja Modi[1], Amritha Nayak[1,2], Andrew Knutsen[1,2], Joelle Sarlls[1], and Carlo Pierpaoli[1]

[1] National Institutes of Health, Bethesda, MD, USA
[2] Center of Neuroregenerative Medicine, Bethesda, MD, USA

Abstract. In this work we propose a novel method to correct echo planar imaging (EPI) distortions in diffusion MRI data acquired with reversed phase encoding directions ("blip-up blip-down" acquisitions). The transformation model is symmetric, diffeomorphic and capable of capturing large deformations. It can take advantage of a structural MRI target and include the contribution of diffusion weighted images, in addition to EPI images acquired without diffusion sensitization. The proposed correction significantly outperform existing strategies, assuring anatomically accurate characterization of the orientation, mean diffusivity, and anisotropy of white matter structures in the human brain.

1 Introduction

Susceptibility and concomitant field distortions in echo planar images (EPI) have been shown to affect diffusion MRI tractography findings [7]. Correction methods have typically involved B_0 field maps [8] or anatomical image targets [12]. The corrections achieved with these methods, however, are suboptimal in areas of large field inhomogeneities, with associated large distortions and large signal pile-ups or expansions. More recently, a methodology which involves the acquisition of the same EPI image twice with reversed phase-encoding gradient originally proposed by [5,4] has been revisited, due to its potential ability to better handle regions of severely piled-up or expanded signals. The original implementation of this method employed the *"line-integral"* principle, which stated that the cumulative signal along a phase encoding line between corresponding points in the up and down image should be equal and that these points should be equidistant to the true anatomical location. The original correction method suffered from numerical instabilities and non-smooth deformation fields because of its $1D$ nature. Andersson et al. proposed a different strategy [1], which aimed to estimate the B_0 map from up and down images together in an image restoration framework. This method, has been released as the *"topup"* tool within the popular FSL package. Elastic or diffemorphic registration based approaches have also been proposed [6,10].

Tools that utilize blip up - blip down acquisitions generally show the potential for superior performance compared to methods using only a single phase encoding direction. However, in many applications to real clinical data, the correction can still be unsatisfactory. This is likely due to inconsistencies between the real data and the underlying physical model, which assumes a stable B_0 field regardless of subject motion, magnetic

P. Golland et al. (Eds.): MICCAI 2014, Part I, LNCS 8673, pp. 218–226, 2014.

drift or heating. Additional artifacts not accounted for, such as Gibbs ringing, ghosts, gradient non-linearities, phase cancellations and the effects of hitting the noise floor, further complicates the problem. In this work, our aim is to propose a robust correction framework for blip-up blip-down acquisitions that suffer less from these limitations.

2 Methodology

The main distinctive properties of the proposed registration framework include:

- *Deformations*: The transformation model is symmetric, diffeomorphic and capable of capturing large deformations with its time varying velocity based model [2].
- *Two deformations*: Instead of one deformation field (and its inverse), we employ two co-dependent deformation fields, which are still almost inverses of each other but with enough flexibility to account for differences in B_0 field between blip up and down acquisitions.
- *Structural image information*: Constraining the flow of the velocity fields composing the deformation fields to pass through a distortion-free structural image at the middle time point is hypothesized to significantly improve registration accuracy.
- *Diffusion image information*: In typical blip-up blip-down correction frameworks, regions homogeneous in $b = 0$ images tend to be freely deformable with insufficient spatial constraints. With other methods, we observed that even with near-perfect alignment between the $b = 0\ s/mm^2$ images and the structural image, DTI-derived directionally encoded color (DEC) maps sometimes reveal anatomically inaccurate corrections. Therefore, the proposed method also employs information extracted form blip up blip down diffusion weighted images to improve anatomical accuracy.
- *Anisotropic deformation regularization*: A new form of deformation regularization is employed to prevent bleeding of small structures into others. Instead of using traditional Gaussian or B-Splines kernels, this method employs a PDE based regularization that results in locally anisotropic smoothing of the deformation fields.

An illustration of the complete correction pipeline is presented in Figure 1. This manuscript will focus on the "DR-BUDDI correction" phase of this pipeline.

2.1 Blip-Up Blip Down Correction

The symmetric registration idea employed in this work originates from the SyN algorithm of Avants used in the popular ANTS registration toolkit [2,3]. The original SyN optimization function formulation aims to register the fixed (I_{up}) and moving image (I_{down}) onto a middle image at $t = 0.5$ as: (without the regularization term)

$$\xi_0 = \int_{\Omega} CC(\overline{I}_{up}(\phi_1(\mathbf{x},0.5)),\overline{I}_{down}(\phi_2(\mathbf{x},0.5)),\mathbf{x})d\Omega \tag{1}$$

where Ω signifies the image domain, CC is the cross-correlation metric, $\overline{I}_{up}$ is the mean subtracted version of I_{up}, $\phi_1(\mathbf{x},t)$ the displacement field that maps the up image to down and $\phi_2(\mathbf{x},t)$ the field mapping the down image to up. Even though theoretically ϕ_1 and ϕ_2 should be of equal norm, the middle images $\overline{I}_{up}(\phi_1(\mathbf{x},0.5))$ and $\overline{I}_{down}(\phi_2(\mathbf{x},0.5)$ can lie anywhere on the hyperplane between the original images and do not necessarily have to be the distortion-free images, which is a single point on this hyperplane.

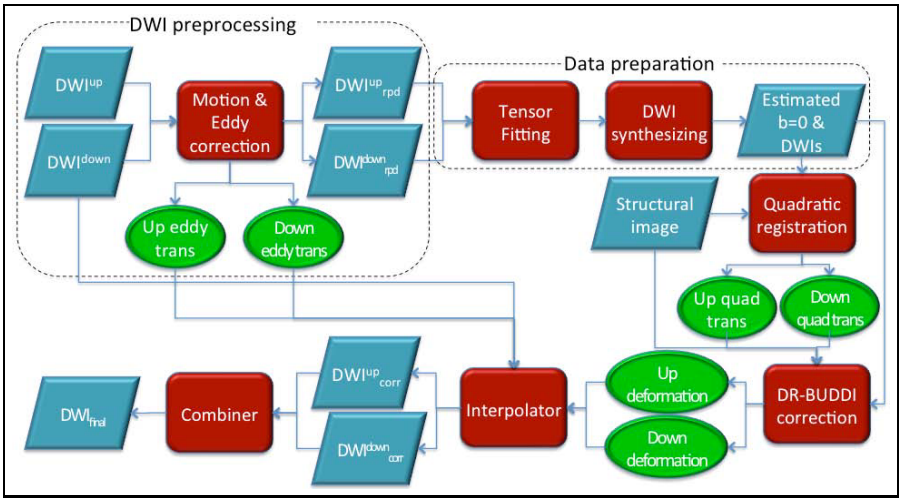

Fig. 1. DWIs are first corrected for motion&eddy currents distortions, then a quick tensor fitting is performed to computed the estimated $b = 0$ images and synthetic DWIs. Quadratic registration is performed with the $b =$ and the structural images to estimate the concomitant fields. Subsequently, the blip up-down correction is performed. All transformations are combined to yield the distortion-free up and down data, which are later combined to produce the final "signal corrected" dataset.

2.2 Metric 1 - Incorporating Geometrical Structural Information

To constrain the flow of displacement velocity fields, the middle images are constrained to pass through a distortion-free structural image $\mathscr{S}$ at the middle time point as:

$$\xi_1 = \int_\Omega \left(CC\left(\overline{I}_{up}\left(\phi_1\left(\mathbf{x}, 0.5\right)\right), \overline{\mathscr{S}}\right) + CC\left(\overline{\mathscr{S}}, \overline{I}_{down}\left(\phi_2\left(\mathbf{x}, 0.5\right)\right)\right)\right) d\Omega \tag{2}$$

This metric encourages the similarity between the structural image and the middle images. Note that it is different from registering the two images to the structural because the displacement fields ϕ_1 and ϕ_2 are of the same norm and can be inter-related (Section 2.4). Therefore, this formulation enforces the up image to go through the structural image at $t = 0.5$ during registration. Displacements can be computed as decribed in [2]:

$$\frac{\partial \xi_1}{\partial \phi_1}(\mathbf{x}) = \frac{2 < I'_{up}, \mathscr{S} >}{< I'_{up}, I'_{up} >< \mathscr{S}, \mathscr{S} >} \times \left(\overline{\mathscr{S}} - \frac{< I'_{up}, \mathscr{S} >}{< I'_{up}, I'_{up} >} \overline{I}'_{up} \right) |\mathscr{J}(\phi_1)| \nabla \overline{I}'_{up} \tag{3}$$

where I'_{up} is $\overline{I}_{up}(\phi_1(\mathbf{x}, 0.5))$ and $< A, B >= \sum_x (A(x) - \mu_A)(B(x) - \mu_B)$. This metric is suitable for calculating geometric displacements but it does not take into account the signal redistribution that should accompany the deformation.

2.3 Metric 2 - Addressing Signal Redistribution

As described by Bowtell [4], once a correspondence between the up and down images is established, signal redistribution can be computed with geometric average as:

$$K = 2\frac{I'_{up}.I'_{down}}{I'_{up} + I'_{down}} \quad , \quad \xi_2 = \int_\Omega CC(\overline{K}, \overline{S}, \mathbf{x}) d\Omega \tag{4}$$

This metric optimizes the similarity between the anatomical and the final signal-redistributed images. Displacements can then be computed with chain-rule as: $\frac{\partial \xi_2}{\partial \phi_1} = \frac{\partial \xi_2}{\partial K}\frac{\partial K}{\partial \phi_1}$.

$$\frac{\partial \xi_2}{\partial K} = \frac{2 < K', \mathscr{S} >}{< K', K' >< \mathscr{S}, \mathscr{S} >}\left(\overline{\mathscr{S}} - \frac{< K', \mathscr{S} >}{< K', K' >}\overline{K}\right) \tag{5}$$

$$\frac{\partial K}{\partial \phi_1} = 2\left(\frac{I'_{down}}{I'_{up}+I'_{down}}\right)^2 |\mathscr{J}(\phi_1)|\nabla \overline{I}'_{up} \quad , \quad \frac{\partial K}{\partial \phi_2} = 2\left(\frac{I'_{up}}{I'_{up}+I'_{down}}\right)^2 |\mathscr{J}(\phi_2)|\nabla \overline{I}'_{down} \tag{6}$$

Metric 2 ensures proper signal redistribution only for the combined image K. The correction of the individual images I_{up} and I_{down} may not be optimal. Therefore, in our algorithm we use a (equally) weighted combination of Metric 1 and 2.

2.4 Constraints and Other Properties of the Registration

Phase Encoding Direction ($\overrightarrow{pe}$): The gradient formulations of Equations 3 and 5 result in free-deformations, which need to be constrained along $\overrightarrow{pe}$ to physically model the system. Let $\mathscr{R}_{up}$ and $\mathscr{R}_{down}$ be the rotational components of the quadratic registration that maps the up and down images to the structural image respectively. Because the diffeomorphic registration is performed on the structural space, $\overrightarrow{pe}$ become oblique. For simplicity, let $\overrightarrow{pe}$ be the y-axis, then the gradients are projected as:

$$\overrightarrow{pe}_{up} = \mathscr{R}_{up}^{\mathbf{T}}\begin{bmatrix}0\\1\\0\end{bmatrix} \quad , \quad \{\frac{\partial \xi_i}{\partial \phi_1}\}_{\overrightarrow{pe}_{up}} = \left(\frac{\partial \xi_i}{\partial \phi_1}\cdot \overrightarrow{pe}_{up}\right)\overrightarrow{pe}_{up}$$

Enforcing Deformation Equality: Theoretically, only one deformation field ϕ_1 and its inverse ϕ_1^{-1} would be sufficient to correct the up and down images. Because of the reasons mentioned in Section 2, we found that employing two co-dependent fields ϕ_1 and ϕ_2 with soft-constraints outperforms the former model. Another term is added to the cost function as: $\xi_i^f = \xi_i + \beta\,||\phi_1 - \phi_2^{-1}||$. Then displacements can be rewritten as:

$$\frac{\partial \xi_i}{\partial \phi_1}^f(\mathbf{x}) = \frac{\partial \xi_i}{\partial \phi_1}(\mathbf{x}) + \frac{\beta}{2}\left(\mathscr{R}_{up}^{\mathbf{T}}\mathscr{R}_{down}\left(\frac{\partial \xi_i}{\partial \phi_2}\right)^{-1}(\mathbf{x}) - \frac{\partial \xi_i}{\partial \phi_1}(\mathbf{x})\right) \tag{7}$$

where β is a continuous user-defined parameter that forces ϕ_1 and ϕ_2^{-1} to be identical when set to one and leave them unconstrained when zero.

2.5 Image Modality for I_{up} and I_{down}

Other methods compute the deformation fields using only non-diffusion weighted $b = 0$ images. Having T_2 contrast, $b = 0$ images are homogeneous in regions such as the brain stem, where different tracts are in close proximity. Using only $b = 0$ images may cause improper distortions of different pathways, sometimes even merging them into a single tract. To address this problem, we perform a vector-image based registration, using synthesized DWIs in addition to the $b = 0$ image. The displacements are computed as a weighted sum over different channels. The number of diffusion weighted images used in registration is a user defined parameter (default=6) with DWIs synthesized with $b = 1000\ s/mm^2$ and gradients generated from electro-static repulsion algorithm.

2.6 Deformation Regularization

Traditionally, regularization of displacement fields have been achieved with convolution of Gaussian or B-Splines kernels. In this work, we preferred to employ an anisotropic filter to avoid blending of neighboring regions such as the brain stem and the surrounding cerebro-spinal fluid. For this purpose, vector valued image regularization framework proposed by Tschumperlé [11] is employed as: $\partial \phi_1^{xyz} / \partial t = trace(\mathbf{TH}^{xyz})$. The Hessian matrix $\mathbf{H}$ is computed from the x, y and z components of the deformation field ϕ_1 and the structure tensor field $\mathbf{T}$ is computed directly from the vector images I'_{up}. Five smoothing iterations are performed for regularizing the fields.

3 Experiments

High-quality, good spatial resolution data (matrix size=128×128, 2mm isotropic, $SNR >$ 30) with very large distortions were collected from one subject on a GE $3T$ scanner with no parallel imaging. Diffusion scans consisted of 10 $b = 0$ and 60 $b = 1100\ s/mm^2$ images. The acquisition was repeated for both phase encode directions; Anterior-Posterior (AP) and Right-Left (RL) with both blips, yielding four datasets: AP_p, AP_m, RL_p, RL_m. The assessment of the quality of the correction was based on the assumption that better corrections should lead to higher similarity between tensor quantities computed from corrected AP and RL data. This assesment was performed both by visual inspection of the corrected $b = 0$ images to the structural image and the directionally encoded color (DEC) maps [9] and analysis of difference images of Fractional Anisotropy (FA) maps. Results from two existing methods, topup and Holland method, were also generated. To validate our hypotheses of Section 2, we also performed tests to show the contributions of using a structural image, using DWIs v.s. using just the $b = 0$ image and using only a single deformation field.

4 Results

Figure 2 displays the distorted up and down $b = 0$ images at two slice levels.

The corrected images with the proposed and existing methods for the first slice level can be found in Figure 3. The proposed algorithm produces very sharp tissue interfaces, an anatomically accurate shape and very similar AP_{corr} and RL_{corr} compared to the other methods. The Holland method does not converge because the phase encode direction of the AP and PA were not collinear in this dataset due to subject motion. The agreement between the FA maps of the corrected AP and RL data is high with the proposed method (Figure 4.a).

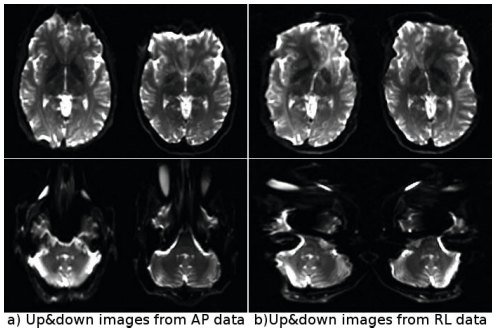

Fig. 2. The original distorted blip up and blip down images for two slice levels, for both the AP and RL data. The distortions in this dataset are very large.

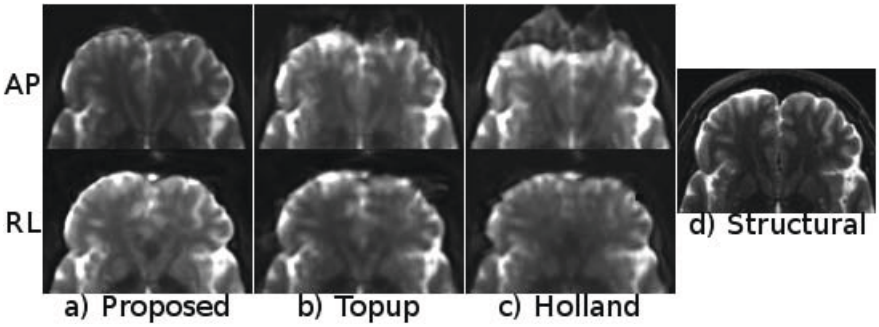

Fig. 3. Corrected b=0 images for a) proposed , b) Topup and c) Holland methods along with the structural image (d), with AP_{corr} (top) and RL_{corr} (bottom), for the first slice level

No structures are present in the AP_{corr}–RL_{corr} difference maps whereas the *topup* method shows misalignement especially around the genu of the Corpus Callosum and internal capsule (Figure 4.b). The median of the absolute value of all brain voxels in the difference image was significantly lower for DR-BUDDI compared to "topup" ($p \simeq 0$ with non-parametric Wilcoxon test).

Figure 5 displays the corrections for the brain stem level. At this level, CSF surrounding the brain stem bleeds into the white matter with all methods with varying degrees. Figure 6 displays the enlarged RL_{corr} DEC maps of this region. With the proposed method, CST and inferior cerebellar peduncles are clearly distinct and show high anisotropy, whereas with the topup method, the two lateral CST bundles are split into three with an artifactual bundle created at the mid-sagittal line. The transverse pontine fibers also bleed into CSF. With Holland's method, the two CST bundles are instead merged into one.

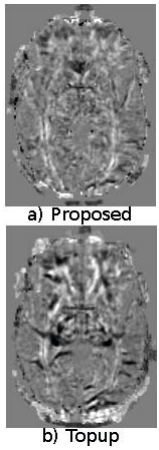

Fig. 4. FA differences

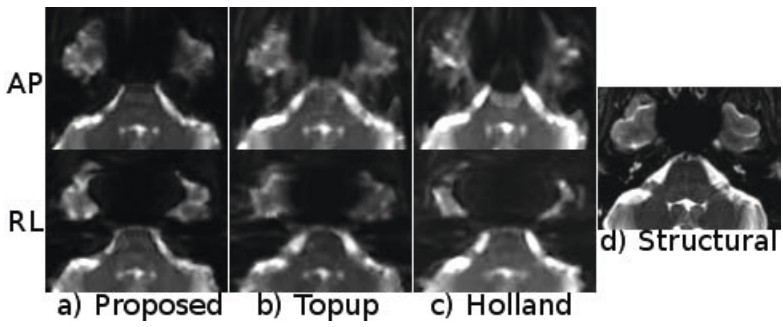

Fig. 5. Corrected images for a) proposed , b) Topup and c) Holland methods along with the structural image for the second slice level

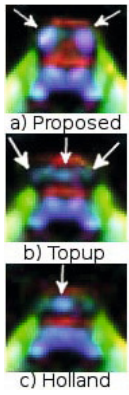

Fig. 6. DEC maps

4.1 Validation of Distinctive Properties

Results presented so far indicates that the proposed method performs better than existing techniques. In this section, we will focus on specific properties of the proposed method and analyze their independent contributions to the overall DR-BUDDI pipeline.

Effect of Using the Structural Image: We analyzed the contribution of using a structural image to guide the flow of the velocity fields. In general we found that the use of the structural image makes the registration more robust and anatomically correct. In Figure 7 we show the same brain used in Figure 3, with and without using a structural image in the registration. The correction obtained without using the structural image shows imperfect correction in the frontal areas.

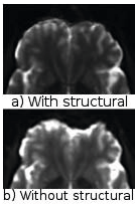

Fig. 7. Structural effect

Effect of Using DWIs: Figure 8 displays the effect of using DWIs with the $b = 0$ image for correction. The Pons is homogeneous in T_2W and using only the $b = 0$ may not contain enough information for a correct registration of pathways within the Pons. In fact, Figure 8.b shows that the Transverse pontine fibers in the ventral aspect of the Pons (arrows) appear broken. Including DWIs within a vector-image registration framework solves this issue (Figure 8.c).

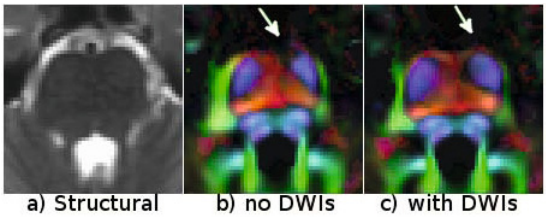

Fig. 8. Effects of using DWIs for correction

Effect of Two Deformations: The effect of using two deformation fields v.s. one was tested by setting β to 1 in Equation 7. Figure 9 displays the displacement fields obtained, at the first slice level, with one and two deformation models. The initial observation is that even with the two deformation model, the displacement fields are almost inverses of each other, which is an implicit property of our system. However, there are differences between ϕ_1 and ϕ also between ϕ_2 and ϕ^{-1}. Two deformation model is able to model a larger displacement with ϕ_1 in the orbito-frontal regions, whereas this was not needed for the moving image as indicated by the similarity of ϕ_2 and ϕ^{-1} in this region. The two deformation model is also able to capture more local details due to the smoothing effect that the other model inherently contains.

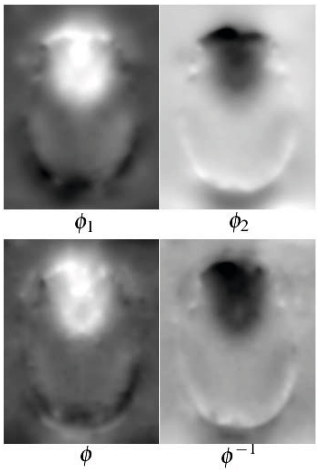

Fig. 9. Displacement fields with two deformation model (top row) and single deformation model (bottom row)

5 Conclusions

In this work, we proposed a novel blip-up blip-down correction method for diffusion MRI. Our method is based on a symmetric, diffeomorphic registration framework, robust at dealing with common issues such as Gibbs ringing, ghosts and motion artifacts. One of our main observations is that it is not sufficient to quality assess only the $b = 0$ s/mm^2 images for diffusion MRI as the DEC maps could reveal spurious, anatomically incorrect features that are not apparent on the former. Therefore, we decided that it was of fundamental importance to make use of DWIs for correction. Using DWIs improved correction quality throughout the white matter but the effects were more pronounced in the brain stem. All the other factors such as the use of a structural MRI, anisotropic regularization and the deformation model also contributed significantly to the overall performance. Future work involves the acquisition of phantom data and creation of simulated models to systematically analyze the limitations of the assumptions underlying blip up/down strategies, such as hitting the noise floor in high $\mathbf{q}$ regimes, and phase cancellations in k-space, which invalidate the mass preservation principle.

References

1. Andersson, J.L., Skare, S., Ashburner, J.: How to correct susceptibility distortions in spin-echo echo-planar images: application to diffusion tensor imaging. NeuroImage 20(2), 870–888 (2003)
2. Avants, B., Epstein, C., Grossman, M., Gee, J.: Symmetric diffeomorphic image registration with cross-correlation: Evaluating automated labeling of elderly and neurodegenerative brain. Medical Image Analysis 12(1), 26–41 (2008)
3. Avants, B., Tustison, N.J., Song, G., Cook, P.A., Klein, A., Gee, J.C.: A reproducible evaluation of ANTs similarity metric performance in brain image registration. NeuroImage 54(3), 2033–2044 (2011)
4. Bowtell, R.W., McIntyre, D.J.O., Commandre, M.J., Glover, P.M., Mansfield, P.: Correction of geometric distortion in echo planar images. In: Proceedings of 2nd Annual Meeting of the SMR, San Francisco, p. 411 (1994)
5. Chang, H., Fitzpatrick, J.M.: A technique for accurate magnetic resonance imaging in the presence of field inhomogeneities. IEEE TMI 11(3), 319–329 (1992)
6. Holland, D., Kuperman, J.M., Dale, A.M.: Efficient correction of inhomogeneous static magnetic field-induced distortion in echo planar imaging. Neuroimage 50, 175–183 (2010)
7. Irfanoglu, M.O., Walker, L., Sarlls, J., Marenco, S., Pierpaoli, C.: Effects of image distortions originating from susceptibility variations and concomitant fields on diffusion MRI tractography results. Neuroimage 15(61), 275–288 (2012)
8. Jezzard, P., Balban, R.: Correction for geometric distortion in echo planar images from B0 field variations. Magnetic Resonance in Medicine 34, 65–73 (1995)
9. Pajevic, S., Pierpaoli, C.: Color schemes to represent the orientation of anisotropic tissues from diffusion tensor data: application to white matter fiber tract mapping in the human brain 42, 526–540 (1999)
10. Ruthotto, L., Kugel, H., Olesch, J., Fischer, B., Modersitzki, J., Burger, M., Wolters, C.H.: Diffeomorphic susceptibility artifact correction of diffusion-weighted magnetic resonance images. Physics in Medicine and Biology 57(18), 5715 (2012)

11. Tschumperlé, D., Deriche, R.: Vector-valued image regularization with PDEs: A common framework for different applications. IEEE Trans. PAMI 27(4), 506–517 (2005)
12. Wu, M., Chang, L.-C., Walker, L., Lemaitre, H., Barnett, A.S., Marenco, S., Pierpaoli, C.: Comparison of EPI distortion correction methods in diffusion tensor MRI using a novel framework. In: Metaxas, D., Axel, L., Fichtinger, G., Székely, G. (eds.) MICCAI 2008, Part II. LNCS, vol. 5242, pp. 321–329. Springer, Heidelberg (2008)